Available online at www.sciencedirect.com
SCIENCE DIRECT®
Journal of Photochemistry and Photobiology A: Chemistry 168 (2004) 97–101
Journal of Photochemistry and Photobiology A:Chemistry
www.elsevier.com/locate/jphotochem

Physical and photocatalytic properties of zinc ferrite doped titania under visible light irradiation

Ping Cheng*, Wei Li, Tianle Zhou, Yanping Jin, Mingyuan Gu

State Key Laboratory of MMCs, Shanghai Jiaotong University, Shanghai 200030, China

Received 18 February 2004; received in revised form 23 April 2004; accepted 19 May 2004
Available online 2 July 2004

Abstract

Visible light responsive zinc ferrite doped titania photocatalyst ($TiO_2(ZnFe_2O_4)$) was prepared by sol–gel method and was calcined at different temperatures. Diffuse reflectance spectroscopy (DRS) results show that the absorption edge of $TiO_2(ZnFe_2O_4)$ has moved to the visible spectrum range in comparison with the undoped titania. The photocatalytic experimental result demonstrates that $TiO_2(ZnFe_2O_4)$ powder can effectively photodegrade methyl orange (MO) under visible light irradiation. Effect of calcination temperature on the photocatalytic activity of $TiO_2(ZnFe_2O_4)$ was also investigated. Zeta potential measurements indicate that the isoelectric point (IEP) of the $TiO_2(ZnFe_2O_4)$ powder shifts to lower pH units with the increase of calcination temperature. Brunauer–Emmett–Teller (BET) surface area decreases with the rise of calcination temperature. It is concluded that the surface charge and BET surface area are the key factors for the higher photoactivity of zinc ferrite doped titania photocatalyst calcined at 400 °C.

Keywords: Photocatalyst; Visible light; Titania; Zinc ferrite; Methyl orange

1. Introduction

In recent years, titania has been widely studied for its wide application in photocatalysis, solar cells and hydrogen production because of its no toxicity, stability in aqueous solution, and no photocorrosion under bandgap illumination [1]. However, titania is a wide bandgap semiconductor (3.03 eV for rutile and 3.18 eV for anatase) and can only absorb about 5% of sunlight in the ultraviolet region, which greatly limits its practical applications. Extensive efforts have been made in the development of titanium oxide photocatalysts that can efficiently utilize solar or indoor light. The approaches include the incorporation of metal ions into titania semiconductor powder or film by ion implantation or chemical doping [2–7]; the introduction of oxygen vacancies by treating a photocatalyst with hydrogen plasma or X-ray irradiation [8,9]; the incorporation of nonmetal ions (e.g. N, C, F, S) into titania crystal lattice [10–13]; the coupling of titania and the other semiconductor with visible light absorption, e.g. CdS, WO_3, and SnO_2 systems by sol–gel process, co-precipitation or simply physical mixing [14–17].

Spinel zinc ferrite is a semiconductor (bandgap 1.9 eV) that has potential application in the conversion of sunlight. However, because of the lower valence band potential and poor property in photoelectric conversion, zinc ferrite cannot be used directly in the photocatalytic destruction of toxic organic compounds [18]. Titania has high photoactivity and superior property in photoelectric conversion, while zinc ferrite is sensitive to visible light. So the coupling of these two semiconductors may become a new type of composite having high utility of sunlight, high photoactivity and high efficiency of photoelectric conversion.

In this paper, zinc ferrite doped titania powder (labeled as $TiO_2(ZnFe_2O_4)$) was prepared by sol–gel method with the aim of extending the light absorption spectrum toward the visible region. The photocatalytic activity under visible light irradiation was evaluated using methyl orange (MO) as a model organic compound. The effect of calcination temperature on the photocatalytic activity of $TiO_2(ZnFe_2O_4)$ has also been studied. The powders calcined at different temperatures were characterized by X-ray diffraction (XRD), diffuse reflectance spectroscopy (DRS) and Brunauer–Emmett–Teller (BET) methods as well as zeta potential measurements. It is found that the $TiO_2(ZnFe_2O_4)$ photocatalyst can effectively photodegrade MO under visi-

* Corresponding author. Tel.: +86-21-62933458; fax: +86-21-62822012.
E-mail address: phedra@sjtu.edu.cn (P. Cheng).

1010-6030/$ – see front matter © 2004 Elsevier B.V. All rights reserved.
doi:10.1016/j.jphotochem.2004.05.018

ble light irradiation and the sample calcined at 400 °C has the higher photoactivity than the ones calcined at 500 and 600 °C.

2. Experimental

2.1. Preparation of zinc ferrite doped titania powders

Zinc ferrite doped titania powder was prepared by sol–gel process and the molar ratio of zinc ferrite to titania is 0.5%. Tetrabutyl titanate, zinc nitrate and ferric nitrate were used as precursors of titania and zinc ferrite, respectively. First, zinc nitrate, ferric nitrate and citric acid in a 1:2:2.5 molar ratio were dissolved together in the ethanol solution to produce a clear solution. The concentration of zinc ion in the solution is 0.15 M. The mixture was vigorously stirred for 2 h and then was diluted to get the required stoichiometric proportion of zinc ferrite to titania.

During the synthesis of titania sol, hydrochloric acid was used as catalyst. The molar ratio of $Ti:H_2O:HCl:C_2H_5OH$ is equal to 1:2.5:1:15. In order to avoid strong hydrolysis reactions, $Ti(OBu^n)_4$ was diluted with half of the prescribed amount of ethanol at first, then water and catalyst dissolved in the remaining ethanol were added dropwise to the ethanolic solution of alkoxide with continuous stirring. Simultaneously, the prescribed diluted zinc ferrite solution was added dropwise to the titania sol. Zinc ferrite/titania sol was obtained after vigorous stirring for several hours. The gel was calcined at the temperature 400, 500 and 600 °C for 2 h, respectively, and then ground into fine powders. For comparison, pure titania and pure zinc ferrite nanopowders were also prepared with the same procedures described previously.

2.2. Measurements and analysis methods

The atomic contents in the final $TiO_2(ZnFe_2O_4)$ powder were determined by an inductively coupled plasma emission (ICP) spectroscopy using an IRIS Advantage 1000 equipment (Thermo Jarrell Ash Corp., USA). The ICP analyses for the final $TiO_2(ZnFe_2O_4)$ powder indicated that the molar ratio of $ZnFe_2O_4$ to TiO_2 is approximately 0.5%. XRD patterns were made in a Rigaku D/max3A diffractometer with Cu Kα radiation over the 2θ range of 10–90° to identify the phase structure of samples. The crystallite size was determined using Scherrer's equation. The DRS spectra of the powders were performed in a TU-1901 dual beam UV-Vis spectrometer, equipped with an integrating sphere attachment for their diffuse reflectance in the range of 230–850 nm. $BaSO_4$ was used as the standard in all measurements. The BET surface area was determined by nitrogen adsorption–desorption isotherm measurements at 77 K on a Micromeritics NOVA 1000 Enitrogen adsorption apparatus. The samples were degassed at 300 °C before each measurement. The pH values of the solutions were measured with a pH meter. Zeta potential measurements were carried out on BI-ZetaPlus (Brookhaven Instruments Corp., USA) which uses the Doppler shift resulting from laser light scatter from the particles to obtain a mobility spectrum. Samples were prepared at solids concentration of 0.5 wt.% in deionized water, 10^{-3} M NaCI electrolyte, and dispersed for 10 min using an ultrasonic probe. After dispersing, the solution was allowed to sediment for 20 min and the agglomerates were removed. The 10^{-2} N HCI and 10^{-2} N NaOH solution were used to adjust pH to the desired values.

2.3. Set-up of photocatalytic reaction

The photocatalytic activities of the samples were evaluated by the decomposition of MO under visible light irradiation at natural pH value. A 250 W high pressure Hg lamp was used as the light source and 1 M $NaNO_2$ solution was utilized for the purpose of excluding ultraviolet radiation. The emission spectrum of the lamp (obtained from the manufacturer) as well as the transmission spectrum of 1 M $NaNO_2$ solution (obtained spectrophotometrically) is presented in Fig. 1(a) and 1(b), respectively. It can be seen that the light from the Hg lamp includes beams from both ultraviolet and visible light regions. After filtered out by 1 M $NaNO_2$ solution, the wavelength of light is larger than 400 nm. The initial concentration of MO in a quartz reaction vessel was fixed at 10 mg/l with a catalyst loading of 5 g/l. The extent of MO decomposition was determined by measuring the absorbance value at approximately 465 nm using a 756MC UV-Vis spectrometer. Prior to illumination, the suspension was magnetically stirred in the dark for 30 min to establish the adsorption–desorption equilibrium at room

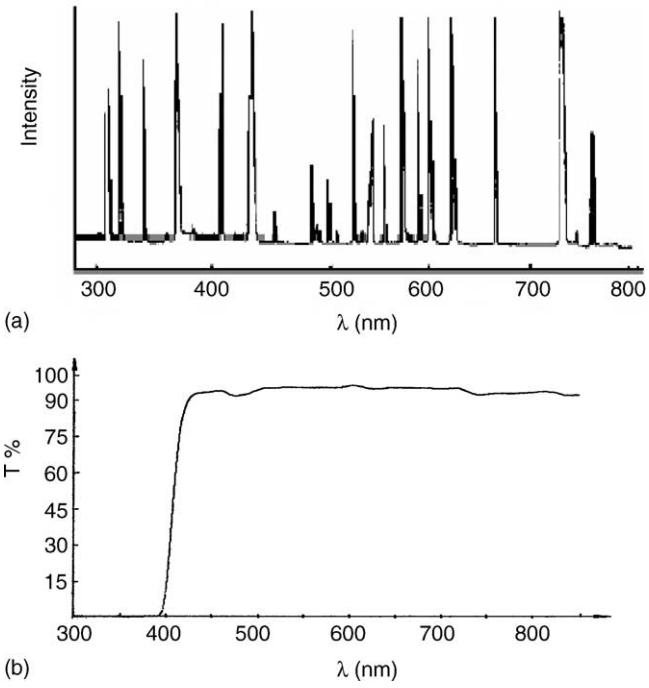

Fig. 1. (a) Emission spectrum of the high pressure mercury lamp; (b) transmission spectrum of 1 M $NaNO_2$ solution.

temperature. During irradiation, stirring was maintained to keep the mixture in suspension. At regular intervals, samples were withdrawn and centrifuged to separate TiO_2 particles for analysis.

3. Results and discussion

3.1. Photodegradation of MO

Fig. 2 shows the effect of calcination temperature on the photocatalytic activity of the $TiO_2(ZnFe_2O_4)$ photocatalysts for the oxidative degradation of MO diluted in distilled water under visible light irradiation ($\lambda > 400$ nm).

After the adsorption equilibrium of MO onto the catalyst was established in the dark, about 51, 10 and 2% of the initial concentration of MO is absorbed onto the $TiO_2(ZnFe_2O_4)$ catalyst for the catalyst calcined at 400, 500 and 600 °C, respectively. Meanwhile, the pH of the suspension was measured immediately after the adsorption equilibrium. It is to be noted that the pH of the solution varied after the MO solution was photodegraded. The extent of variation depends on the irradiating time. However, in the entire time range studied, variation found were very little. In addition, at the end of the photocatalytic reaction, pH was recorded and the difference was found negligible. As shown in Fig. 3, the natural pH values of 4.0, 5.7 and 6.1 were obtained for the sample calcined at 400, 500 and 600 °C, respectively. The increase of the pH value with the increase of calcination temperature is due to the reduction of surface acidic groups in the $TiO_2(ZnFe_2O_4)$ powder, which were introduced during the preparation.

A blank experiment in the absence of irradiation but with $TiO_2(ZnFe_2O_4)$ demonstrates that no MO degradation occurs. Another blank experiment in the absence of $TiO_2(ZnFe_2O_4)$ but under irradiation shows that MO cannot be degraded under the present experimental condition.

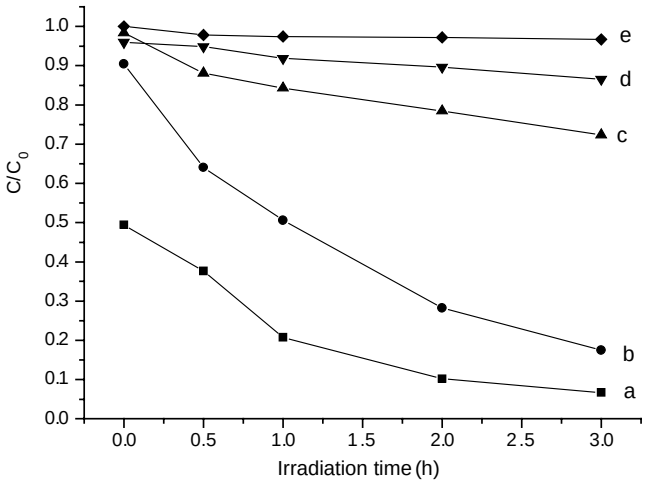

Fig. 2. The effect of calcination temperature on the photocatalytic activity of $TiO_2(ZnFe_2O_4)$ for the degradation of MO under visible light irradiation: (a) 400 °C; (b) 500 °C; (c) 600 °C; (d) TiO_2 500 °C; (e) $ZnFe_2O_4$ 500 °C.

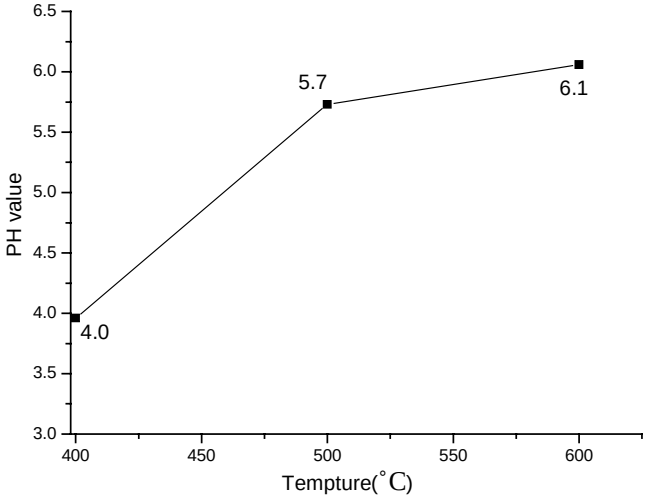

Fig. 3. The variation of natural pH value for $TiO_2(ZnFe_2O_4)$ suspension as a function of calcination temperature.

It can be seen that the photocatalytic degradation of MO proceeded on the $TiO_2(ZnFe_2O_4)$ photocatalyst under visible light irradiation (a–c). After 3 h photodegradation reaction excited by visible light, 93% methyl orange were destroyed on the $TiO_2(ZnFe_2O_4)$ samples, while only 13% methyl orange were degraded on pure TiO_2 (d). The degradation of methyl orange on pure TiO_2 under visible light irradiation is attributed to the photosensitization process [19]. Anatase titania cannot be directly excitated by visible light due to its 3.2 eV bandgap, but the photobleaching reaction still occurred under TiO_2/dye/visible-light system due to dye molecule acting as photosensitizer. The electron from the excited dye molecule was injected into the conduction band (CB) of the TiO_2, and the cation radical formed at the dye surface quickly undergoes degradation reaction. Moreover, the $TiO_2(ZnFe_2O_4)$ powder calcined at 400 °C showed a higher photocatalytic reactivity in comparison with the samples calcined at 500 and 600 °C. It is found that the photoactivity is closely related to the dark adsorption amount of MO onto the samples. The more MO is absorbed onto the catalyst, the higher is the photoactivity.

3.2. XRD and BET results

Fig. 4 illustrates the XRD patterns of $TiO_2(ZnFe_2O_4)$ calcined at 400, 500 and 600 °C. It can be seen that the diffraction peaks at corresponding diffraction angles of anatase phase become much sharper when the temperature increase from 400 to 600 °C. There appear no peaks for rutile in all samples. It means that the phase transformation from anatase to rutile did not take place when $TiO_2(ZnFe_2O_4)$ powder was calcined at temperatures below 600 °C. Meanwhile, zinc ferrite peaks can be detected in the samples calcined at 500 and 600 °C although they are very weak.

The crystallite size of powders was determined from the broadening of corresponding X-ray diffraction peaks by

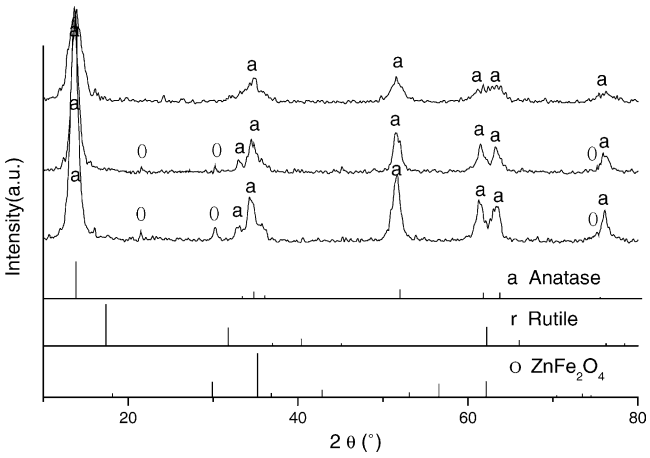

Fig. 4. XRD patterns of $TiO_2(ZnFe_2O_4)$ calcined at various temperatures: (a) 400 °C; (b) 500 °C; (c) 600 °C.

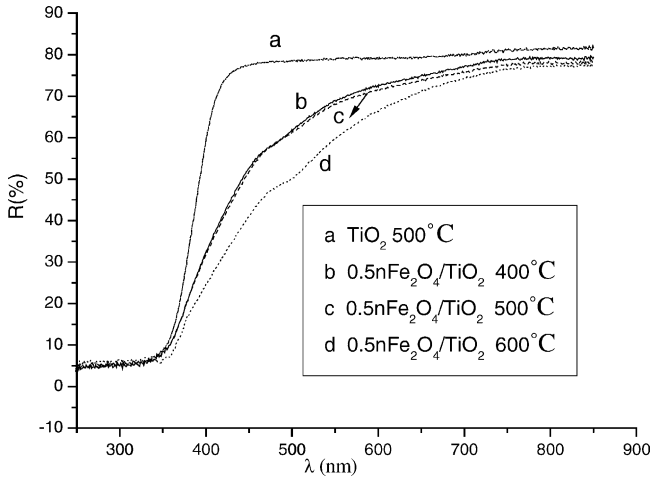

Fig. 5. DRS spectra for $TiO_2(ZnFe_2O_4)$ calcined at various temperatures.

using Scherrer's formula $D = K\lambda/\beta\cos\theta$, where λ is the wavelength of the X-ray radiation ($\lambda = 0.15418$ nm), K the Scherrer constant ($K = 0.9$), θ the X-ray diffraction peak and β the full-width at half-maximum (FWHM) of the (1 0 1) plane (in radians), which is corrected for the instrumental broadening ($\beta_0 = 0.00122$ rad) prior to calculation of its real particle size broadening [20]. The estimated anatase grain sizes of $TiO_2(ZnFe_2O_4)$ calcinated at 400, 500 and 600 °C were 7.35, 11.97 and 14.62 nm, respectively (shown in Table 1).

The BET specific surface areas of $TiO_2(ZnFe_2O_4)$ powders calcined at different temperatures are also listed in Table 1. The sample treated at 400 °C shows specific surface areas of 96 m^2/g. However, by increasing the thermal treatment to 500 and 600 °C, the surface area notably diminishes to 47 and 15 m^2/g, respectively. This is obviously due to progressive aggregation of small crystallites into larger particles. It is concluded that the higher BET surface area of $TiO_2(ZnFe_2O_4)$ photocatalyst calcined at 400 °C provides a larger adsorption site on the catalyst surface for MO, therefore the higher is the photoactivity. Similar findings were also reported. Photocatalysts having a larger BET surface area have a higher conversion for organic compounds in the gaseous phase and phenol in the aqueous phase [21,22].

3.3. DRS results

Fig. 5 shows the reflectance spectra of $TiO_2(ZnFe_2O_4)$ powders calcinated at 400, 500 and 600 °C and pure TiO_2. The energy bandgaps are 2.86, 2.82 and 2.70 eV for $TiO_2(ZnFe_2O_4)$ powders calcinated at 400, 500 and 600 °C, respectively, and 3.18 eV for pure TiO_2. It can been seen that an redshift in $TiO_2(ZnFe_2O_4)$ powders is obtained in comparison with pure titania. This means that the $TiO_2(ZnFe_2O_4)$ powder is sensitive to visible light, which accounts for the photoactivity of $TiO_2(ZnFe_2O_4)$ under visible light irradiation.

Table 1
Characteristics of the $TiO_2(ZnFe_2O_4)$ photocatalyst calcined at different temperatures

Temperature (°C)	Crystal size (nm)	Crystal phase	BET surface area (m^2/g)
400	7.35	Anatase	96
500	11.97	Anatase	47
600	14.62	Anatase	15

Furthermore, the redshift of the absorption edge is also seen in the $TiO_2(ZnFe_2O_4)$ powder when the annealing temperature increases from 400 to 600 °C. It has been reported that the blueshift in the absorption band edge was claimed as a consequence of exciton confinement with decreasing particle size (the so-called quantum size effect) in titania [23]. In the present study, the grain size of anatase titania increases from 7.35 to 14.62 nm when the calcination temperature increases from 400 to 600 °C. So the redshift of the absorption edge from 400 to 600 °C is believed to be mainly due to the exciton confinement effect of zinc ferrite particles embedded in the titania matrix.

It is generally accepted that the redshift of absorption band can increase photon numbers by extending the energy range of photoexcitation, which can be absorbed by catalyst and utilized for the photocatalytic reaction. In this study, although the $TiO_2(ZnFe_2O_4)$ catalyst calcined at 400 °C has a smaller absorption edge in the visible region, its photoactivity for MO degradation is higher. It can be inferred that light absorption is not the only factor that determines the visible light photoactivity of $TiO_2(ZnFe_2O_4)$ catalysts calcined at different temperatures.

3.4. Zeta potential

Fig. 6 shows the zeta potential data for $TiO_2(ZnFe_2O_4)$ photocatalyst calcined at different temperatures. The results show a clear difference in isoelectric point (IEP) between the three samples. The isoelectric point of $TiO_2(ZnFe_2O_4)$ photocatalyst calcined at 400, 500 and 600 °C is 6.6, 5.8

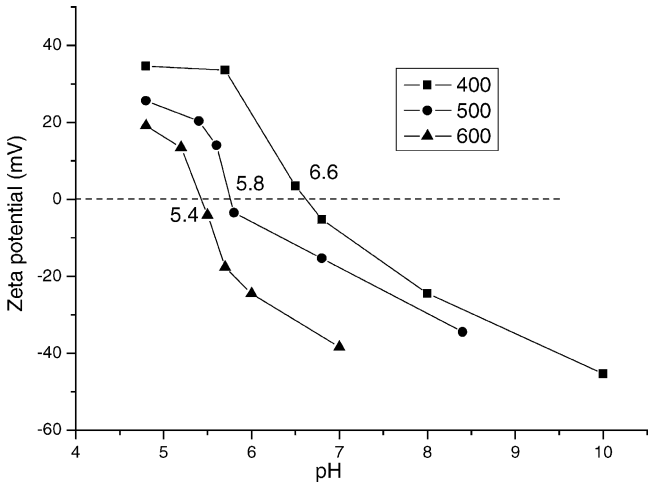

Fig. 6. Zeta potential of $TiO_2(ZnFe_2O_4)$ powder as a function of pH value.

and 5.4 pH units, respectively. As can be seen, the IEP of $TiO_2(ZnFe_2O_4)$ powders shifts to lower pH values with the increase of calcination temperature. When pH is less than the IEP, the zeta potential for $TiO_2(ZnFe_2O_4)$ is larger than 0 mV, which means the surface of $TiO_2(ZnFe_2O_4)$ powder is of positive charge. As previously shown in Fig. 3, the natural pH values for the sample calcined at 400, 500 and 600 °C are 4.0, 5.7 and 6.1, respectively. So, for the catalyst calcined at 400 °C, the pH of 4.0 is far below the IEP of 6.6 and the catalyst is positively charged; However, for the catalyst at 600 °C, the pH of 6.1 is above the IEP of 5.4 and a negative zeta potential is obtained, which implies the catalyst is negatively charged; As for the powder at 500 °C, 5.7 is approximately equal to 5.8 and the obtained zeta potential is zero, which indicates a neutral surface for the sample.

Consequently, for the sample calcined at 400 °C, the positively charged $TiO_2(ZnFe_2O_4)$ offers a suitable surface for adsorption of MO anion [24]. However, increasing the calcination temperature gradually increases the electrostatic repulsion between the MO anion ($pK_1 = 3.46$) and the oxide surface, which reduces adsorption of MO onto the catalyst. Therefore, the drastic decrease in degradation of MO on $TiO_2(ZnFe_2O_4)$ photocatalyst can be seen when the calcination temperature increases from 400 to 600 °C.

4. Conclusion

1. The zinc ferrite doped titania photocatalyst was prepared by sol–gel method. DRS results show that the absorption edge of the photocatalyst has moved to the visible spectrum range, and a large redshift occurs in comparison with the undoped titania. The photocatalytic experiment for the degradation of MO indicates that the $TiO_2(ZnFe_2O_4)$ powders can effectively photodegrade MO under visible light irradiation, while the reactivity was hardly observed on the undoped original TiO_2 or pure $ZnFe_2O_4$ photocatalyst. The photoactivity of $TiO_2(ZnFe_2O_4)$ decreases with the increase of calcination temperature in the range of 400–600 °C.
2. With the increase of calcination temperature, not only the decrease of BET surface area, but also the change in IEP of the photocatalyst occurs. Both the surface charge and the BET surface area affect the adsorption of MO on the $TiO_2(ZnFe_2O_4)$ photocatalyst, therefore account for the higher photoactivity of $TiO_2(ZnFe_2O_4)$ calcined at 400 °C.

Acknowledgements

This work was financially supported by the National Natural Science Foundation of China and the Hi-Tech Research and Development Program (973 Program) of China.

References

[1] D.W. Bahnemann, J. Cunningham, M.A. Fox, E. Pelizzetti, P. Pichat, N. Serpone, in: G.R. Helz, R.G. Zepp, D.G. Crosby (Eds.), Aquatic and Surface Photochemistry, Lewis Publishers, Boca Raton, 1994.
[2] M. Anpo, M. Takeuchi, J. Catal. 216 (2003) 506–516.
[3] D. Dvoranová, V. Brezová, M. Mazúr, M.A. Malati, Appl. Catal. B Environ. 37 (2002) 91.
[4] Y. Takahashi, S. Murata, H. Arakawa, J. Photochem. Photobiol. A Chem. 145 (2001) 135.
[5] Y. Xie, C. Yuan, Appl. Catal. B 46 (2003) 251–259.
[6] K. Zakrzewska, M. Radecka, A. Kruk, W. Osuch, Solid State Ion. 157 (2003) 349–356.
[7] J.-W. Yoon, T. Sasaki, N. Koshizaki, et al., Scripta Mater. 44 (2001) 1865–1868.
[8] I. Nakamura, N. Negishi, S. Kutsuna, T. Ihara, S. Sugihara, K. Takeuchi, J. Mol. Catal. A Chem. 161 (2000) 205.
[9] S. Iimura, H. Teduka, A. Nakagawa, S. Yoshihara, T. Shirakashi, Electrochemistry 69 (5) (2001) 324.
[10] R. Asahi, T. Morikawa, T. Ohwaki, et al., Science 293 (2001) 269.
[11] S.U.M. Khan, M. Al-Shahry, et al., Science 297 (2002) 2243.
[12] A. Hattori, H. Tada, J. Sol-Gel Sci. Technol. 22 (2001) 47–52.
[13] T. Umebayashi, T. Yamaki, H. Itoh, K. Asai, Appl. Phys. Lett. 81 (2002) 454.
[14] K.R. Gopidas, M. Bohorquez, P.V. Kamat, J. Phys. Chem. 94 (1990) 6435.
[15] X. Li, F. Li, C. Yang, W. Ge, J. Photochem. Photobiol. A Chem. 141 (2001) 209.
[16] A. Fuerte, M.D. Hernández-Alonso, A.J. Maira, A. Martínez-Arias, M. Fernández-García, J.C. Conesa, J. Soria, G. Munuera, J. Catal. 212 (2002) 1.
[17] C. Wang, J. Zhao, X. Wang, B. Bai, G. Sheng, P. Peng, J. Fu, Appl. Catal. B Environ. 39 (2002) 269.
[18] M.A. Valenzuela, P. Bosch, J. Jiménez-Becerrill, O. Quiroz, A.I. Páez, J. Photochem. Photobiol. A 148 (2002) 177–182.
[19] G.J. de, A.A. Soler-Illia, R.J. Candel, A.E. Regazzoni, M.A. Blesa, Chem. Mater. 9 (1997) 184.
[20] J.P. Rainho, J. Rocha, L.D. Carlos, J. Mater. Res. 16 (2001) 2369.
[21] M. Mikula, V. Brezova, M. Ceppan, L. Pach, L. Karpinsky, J. Mater. Sci. Lett. 14 (1995) 615.
[22] X. Deng, Y. Yue, Z. Gao, Appl. Catal. B Environ. 39 (2002) 135.
[23] L.D. Zhang, J.M. Mou, Nanometer Materials Science, Liaoning Press of Science and Technology, Shenyang, 1994.
[24] W. Cun, Z. Jincai, W. Xinming, M. Bixian, S. Guoying, P. Ping'an, F. Jiamo, Appl. Catal. B Environ. 39 (2002) 269–279.